Electron Spin Resonance and Neutron Diffraction Studies of $Nd_{0.5-x}Pr_xSr_{0.5}MnO_3$ ($x = 0.125, 0.25$)

C. Autret-Lambert,*,† Z. Jirak,‡ M. Gervais,† N. Poirot,† F. Gervais,† N. Raimboux,§ P. Simon,§ F. Bourée,|| and G. André||

LEMA, UMR 6157 CNRS-CEA, Faculté des Sciences et Techniques, Université François Rabelais, Parc de Grandmont, 37200 Tours, France, Institute of Physics ACSR, Cukrovarnicka 10, 162 53 Prague 6, Czech Republic, CRMHT, UPR4212 CNRS, 45071 Orléans Cedex 02, France, and Laboratoire Léon Brillouin, CEA-CNRS Saclay, 91191 Gif-sur-Yvette Cedex, France

Received March 6, 2007. Revised Manuscript Received July 2, 2007

Effects of Pr substitution on the magnetic properties of perovskite manganite $Nd_{0.5}Sr_{0.5}MnO_3$ have been investigated by measurements of electron spin resonance, magnetization, and powder neutron diffraction. These experiments evidence a complex phase-segregated state at low temperatures and coexistence of different ferromagnetic (FM) and antiferromagnetic (AFM) arrangements. Four temperature regions are distinguished, similar for both studied samples $Nd_{0.5-x}Pr_xSr_{0.5}MnO_3$ ($x = 0.125, 0.25$). Around the room temperature and above there is a region of a single orthorhombic perovskite *Ibmm* phase of paramagnetic (PM) state, where the first signatures for FM clusters can be indicated in the electron spin resonance spectra below ~1.1 T_C ($T_C = 260$ K). Between T_C and T_{C2} (230 K for $x = 0.25$), a new tetragonal perovskite *I*4/*mcm* phase of FM long range order is formed at the expense of the PM orthorhombic phase. Below T_{C2}, the FM order is established in both crystallographic phases, and the amount of the tetragonal phase for $x = 0.25$ achieves a maximum close to 45% of the sample. Finally, below ~160 K, strongly distorted perovskite domains with the CE and A-type kinds of AFM order ($T_N = 150$ K for $x = 0.25$) are segregated while the orthorhombic FM phase quickly vanishes. At the lowest temperatures, the two structurally distorted AFM domains make up 72% of the $x = 0.25$ sample, and the remaining 28% belongs to the tetragonal FM domains.

Introduction

Manganites $Ln_{1-x}AE_xMnO_3$ (Ln is a trivalent lanthanide, AE is a divalent alkaline earth) show a rich phase diagram depending on the doping, temperature, and applied external field. Special attention is attracted to regions of intrinsic phase coexistence. The understanding of physics associated with such phase separation in manganites is still a matter of discussion and gives rise to special motivations for fundamental and applied research activities.[1,2]

An interesting example of this phase separation is the coexistence of charge and orbitally (CO) ordered antiferromagnetic (AFM) phase with a structurally distinct ferromagnetic metallic (FMM) phase. The prototypes of CO phase are the $x = 0.5$ manganites $Pr_{0.5}Ca_{0.5}MnO_3$,[3] $La_{0.5}Ca_{0.5}MnO_3$,[4] and $Nd_{0.5}Sr_{0.5}MnO_3$.[5,6] Their state is associated with the CE-type magnetic order, which is described like ferromagnetic (FM) zigzag chains in the base plane coupled antiferromagnetically to each other. This kind of arrangement can be understood considering a checkerboard distribution of the Mn^{3+} and Mn^{4+} valences as proposed originally by Goodenough and supported later by powder neutron diffraction studies.[4,7,8] However, this classical model of Mn^{3+}/Mn^{4+} CO ordering is recently debated.[9−11] Indeed, from single-crystal neutron diffraction experiments, the low-temperature phase is alternatively described as formed by dimers of Mn ions having a very similar oxygen octahedral environment and thus the same valence $Mn^{3.5+}$. Instead of the charge disproportionation, a formation of Zener polarons is proposed as an electronic localization mechanism. Nevertheless, some questions remain open.

Recently, a new mechanism of colossal magnetoresistance was based on the multicritical fluctuations between the FM metallic and the CO insulating state occurring near $x = 0.5$.[12] Then, the enhanced fluctuations near this multicritical point

* Corresponding author. E-mail address: cecile.autret@univ-tours.fr.
† Université François Rabelais.
‡ Institute of Physics ACSR.
§ CRMHT, UPR4212 CNRS.
|| CEA-CNRS Saclay.

(1) For a review, see, for example, *Colossal Magnetoresistive Oxides*; Tokura, Y., Ed.; Gordon and Breach: Tokyo, 1999.
(2) For a review, see, for example, Dagotto, E.; Hotta, T.; Moreo, A. *Phys. Rep.* **2001**, *344*, 1.
(3) Tomioka, Y.; Asamitsu, A.; Kuwahara, H.; Moritomo, Y.; Tokura, Y. *Phys. Rev. B* **1996**, *53*, R1689.
(4) Radaelli, P. G.; Cox, D. E.; Marezio, M.; Cheong, S.-W. *Phys. Rev. B* **1997**, *55*, 3015.
(5) Kuwahara, H.; Tomioka, Y.; Asamitsu, A.; Moritomo, Y. T.; Tokura, Y. *Science* **1995**, *270*, 961.
(6) Woodward, P. M.; Cox, D. E.; Vogt, T.; Rao, C. N. R.; Cheetham, A. K. *Chem. Mater.* **1999**, *11*, 3528.
(7) Damay, F.; Martin, C.; Hervieu, M.; Maignan, A.; Raveau, B. *J. Magn. Magn. Mater.* **1998**, *184*, 71.
(8) Jirák, Z.; Damay, F.; Hervieu, M.; Martin, C.; Raveau, B.; André, G.; Bourée, F. *Phys. Rev. B* **2000**, *61*, 1181.
(9) Daoud-Aladine, A.; Rodríguez-Carvajal, J.; Pinsard-Gaudart, L.; Fernández-Díaz, M. T.; Revcolevschi, A. *Phys. Rev. Lett.* **2002**, *89*, 097205.
(10) Coey, M. *Nature (London)* **2004**, *430*, 155.
(11) Herrero-Martin, J.; Garcia, J.; Subias, G., Blasco, J.; Concepcion-Sanchez, M. *Phys. Rev. B* **2004**, *70*, 024408.
(12) Murakami, S.; Nagaosa, N. *Phys. Rev. Lett.* **2003**, *90*, 197201.

10.1021/cm070628+ CCC: $37.00
Published on Web 09/26/2007

trigger off a giant response to the external magnetic field. In these materials, the disorder appears to play an important role, which leads to an inhomogeneous state with competing and coexisting phases observed experimentally.[13−15] In the perovskite structure, the disorder is defined by the variance of the size of the Ln and AE cations. The resistivity is determined by the percolating paths, which are sensitive to the amount of metallic regions, leading to a large change of the resistivity under an external applied field. So, the percolation origin of the CMR is phenomenologically proposed.[15,16]

The compound $Nd_{0.5}Sr_{0.5}MnO_3$ can be taken as a marked case of the multiphase coexistence. It shows a transition from the paramagnetic insulator to the FMM state at 255 K and then undergoes a structural distortion associated with charge ordering and onset of antiferromagnetism at 160 K.[5] A number of experiments indicate that the low-temperature phase is in fact nonuniform. The residual FMM regions were evidenced by transmission electron microscopy and nuclear magnetic resonance.[17] Moreover, using neutron diffraction,[6,18] two different AFM arrangements were found in the structurally distorted phase: the majority were CE-type associated with the charge ordering, and the minority were A-type, described previously as a ground state in an analogous manganite $Pr_{0.5}Sr_{0.5}MnO_3$.[7] The latter compound shows also a FMM state on cooling below 265 K before it transforms at 135 K to the A-type AFM metallic state with traces of FMM regions.[19] The local disorder that is at the root of phase separation in $Nd_{0.5}Sr_{0.5}MnO_3$ and $Pr_{0.5}Sr_{0.5}MnO_3$ will be increased obviously in their solid solutions. We report here the study of $Nd_{0.375}Pr_{0.125}Sr_{0.5}MnO_3$ and $Nd_{0.25}Pr_{0.25}Sr_{0.5}MnO_3$ with the aim to study the evolution of the three magnetic states, FM, CE, and A-type AFM, with the temperature.

Experiments

The polycrystalline samples $Nd_{0.5-x}Pr_xSr_{0.5}MnO_3$ ($x = 0.125$, 0.25) were prepared by an organic gel-assisted citrate process. The gel obtained was calcined at 750 °C for 5 h to give an intermediate black powder. The mixed powder was pressed into pellets and heated at 1250 °C for 12 h in air.

The powder X-ray patterns were recorded at room temperature by using a D8 diffractometer ($\theta-\theta$) with a Cu Kα radiation. Neutron powder diffraction (NPD) experiments were performed at the Orphée Reactor, Léon Brillouin Laboratory (Saclay-France), on the two-axis diffractometers 3T2 ($\lambda = 1.225$ Å) and G4.1 ($\lambda = 2.4266$ Å). The temperature dependence of the magnetic and crystalline structures was studied by recording data on cooling from 300 to 1.5 K by 10 K steps on G4.1 (in the angular range $12° < 2\theta < 92°$ by step of 0.1°). A measurement ($6° < 2\theta < 125°$ by step of 0.05°) has been done on 3T2 at 300 K. The nuclear and magnetic structures were refined by the Rietveld method, using the program Fullprof.[20] The oxygen ratio was determined by NPD. It is equal to 3 in the limit of accuracy of the technique.

The magnetic susceptibility (χ) was measured with a Manics Faraday-based magneto-susceptometer in the range 80 to 300 K under a magnetic field of 1 T.

Electron spin resonance (ESR) measurements in the X band (≈9.5 GHz) were performed using a Bruker ER 200-SRC spectrometer with a continuous nitrogen flow apparatus, upon heating in the range 130−330 K. A small amount of loose packed powder (1 mg) is sufficient and was placed at the bottom of a cavity. The EMR spectra parameters were calculated with respect to α,α-diphenyl-β-picryl hydrazyl line (DPPH is used as the *g* marker): g_{eff}, line width, ΔH_{pp}, and double integrated intensity (DIN) were analyzed.

Results and Discussion

1. Structural Determination. Powder X-ray diffraction patterns of $Nd_{0.5-x}Pr_xSr_{0.5}MnO_3$ ($x = 0.125$, 0.25) at room temperature revealed a single perovskite phase. The structure for $x = 0.25$ ($Nd_{0.25}Pr_{0.25}Sr_{0.5}MnO_3$) was refined using high-resolution data from the 3T2 neutron diffractometer. The fit confirms the structure of orthorhombic symmetry *Ibmm*, identical to that reported for the $Nd_{0.5}Sr_{0.5}MnO_3$ oxide, $x = 0$.[21−22] This structure is characterized by a tilt of octahedra around the *b* axis (in Glazer's classification $a^-a^-c^0$, denoting an antiphase tilting about the pseudocubic [110] direction). The orthorhombic unit cell is related to the simple cubic perovskite lattice parameter ($a_p \approx 3.8$ Å) by $a \approx b \approx a_p\sqrt{2}$ and $c \approx 2a_p$.

Observed and simulated patterns for $x = 0.25$ are given in Figure 1. The reliability factors are $R_p = 2.03\%$, $R_{wp} = 2.54\%$, $R_{Bragg} = 4.4\%$, and $\chi^2 = 1.81$. The final refinements are satisfactory and do not show any extra peaks due to an impurity. The Nd, Pr, and Sr cations are randomly settled at the same crystallographic site. The unit cell volume monotonously increases from 226.9 Å^3 for $x = 0$ to 227.3 Å^3 for $x = 0.25$, which arises from the fact that the Pr^{3+} ions are slightly larger than those of Nd^{3+}. The respective radii are 1.179 Å and 1.163 Å.[23] Thus, the average A-site cation radius $\langle r_A \rangle$ ($\langle r_A \rangle = \sum y_i r_i$ calculated from the standard ionic radii) increases with *x* from 1.2365 Å to 1.2405 Å, whereas the deviation from this relation due to the size mismatch of A-site cations, quantified by the size variance parameter $\sigma^2 = \sum y_i r_i^2 - \langle r_A \rangle^2$, remains nearly constant. The octahedral coordination of Mn with oxygen is only slightly distorted with the two $Mn-O_{apical}$ (along the *c* axis) becoming shorter than the four $Mn-O_{equatorial}$ in the *ab* plane, 1.9305(4) Å and 1.9367(1) Å, respectively for $x = 0.25$. The tilting angle of MnO_6 octahedra around the *b* axis is ±8.3° as follows from the calculated $Mn-O_{apical}-Mn$ angle 163.44(2)°. With respect to the *Ibmm* symmetry of the $x = 0.25$

(13) Mori, S., Chen, C. H.; Cheong, S-W. *Phys. Rev. Lett.* **1998**, *81*, 3972.
(14) Uehara, M.; Mori, S., Chen, C. H.; Cheong, S.-W. *Nature (London)* **1999**, *399*, 560.
(15) Moreo, A.; unoki, S.; Dagotto, E. *Science* **2004**, *283*, 1999.
(16) Burgy, J.; Mayr, M.; Martin-Mayor, V.; Moreo, A.; Dagotto, E. *Phys. Rev. Lett.* **2001**, *87*, 277202.
(17) Fukumoto, N.; Mori, S.; Yamamoto, N.; Moritomo, Y.; Katsufuji, T.; Chen, C. H.; Cheong, S.-W. *Phys. Rev. B* **1999**, 60, 12963.
(18) Ritter, C.; Mahendiran, R.; Ibarra, M. R.; Morellon, L.; Maignan, A.; Raveau, B.; Rao, *Phys. Rev. B* **2000**, *61*, R9229.
(19) Hejtmanek, J.; Pollert, E.; Jirak, Z.; Sedmidubsky, D.; Strejc, A.; Maignan, A.; Chapter Martin, Hardy, V.; Kuzel, R.; Tomioka, Y. *Phys. Rev. B* **2002**, *66*, 014426.
(20) Rodriguez-Carjaval, J. *Physica B* **1993**, *192*, 55.
(21) Autret, C.; Gervais, M.; Gervais, F.; Simon, P.; Raimboux, N. *Solid State Sci.* **2004**, *6*, 815.
(22) Autret-Lambert, C.; Gervais, M.; Gervais, F.; Raimboux, N.; Simon, P. *Solid State Sci.* **2005**, *7*, 1035.
(23) Shannon, D. *Acta Crystallogr., Sect. A* **1976**, *32*, 751.

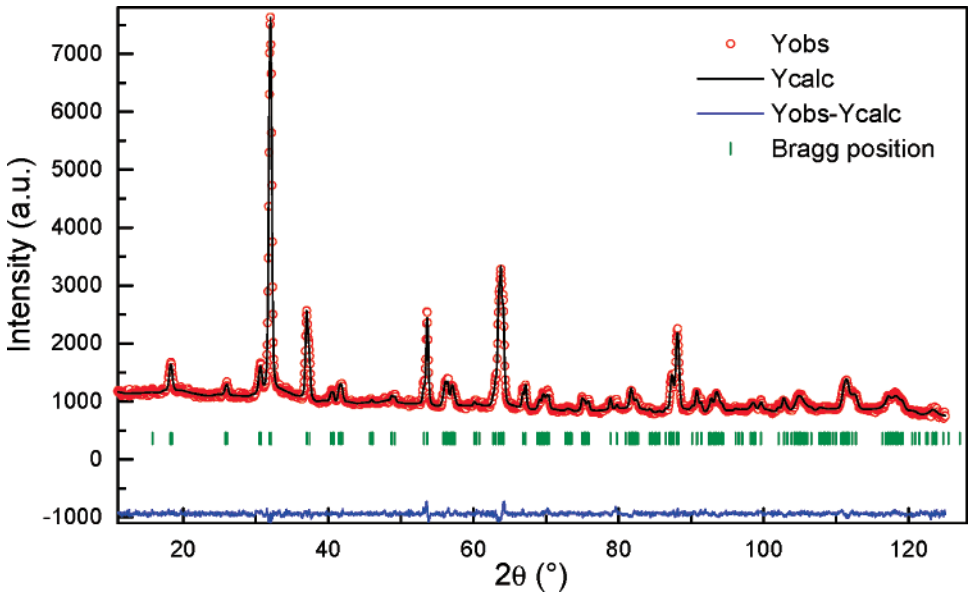

Figure 1. Final refinement with experimental (○), calculated (−), and difference NPD patterns of $Nd_{0.25}Pr_{0.25}Sr_{0.5}MnO_3$ at room temperature ($\lambda = 1.2244$ Å). The position of the Bragg peaks of the *Ibmm* phase is marked below.

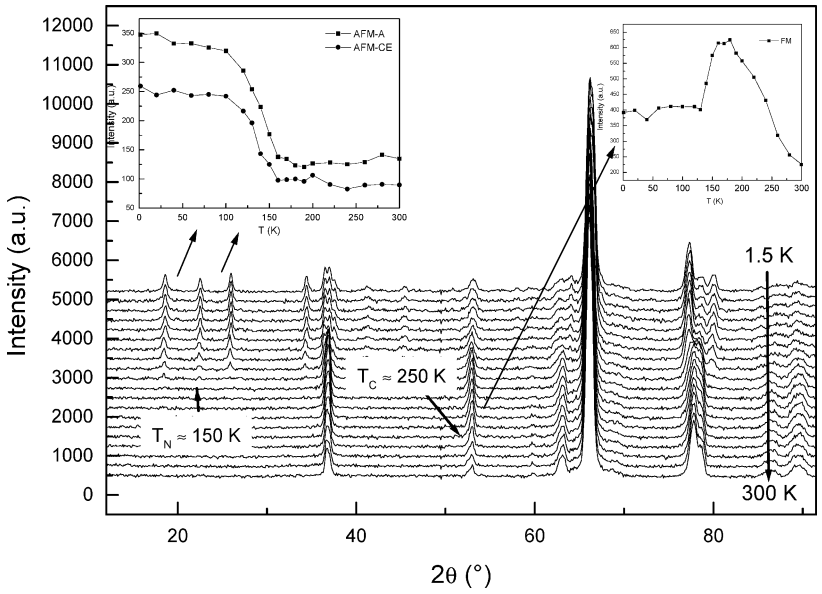

Figure 2. Temperature dependence of the NPD patterns registered on the G4.1 diffractometer from 1.5 to 300 K for $Nd_{0.25}Pr_{0.25}Sr_{0.5}MnO_3$. Insets give the integrated intensities versus *T* of three peaks characteristic of AFM CE-A (left inset) and FM (right inset).

sample, it is worth mentioning that the $Pr_{0.5}Sr_{0.5}MnO_3$ oxide ($x = 0.5$) possesses the tetragonal *I*4/*mcm* symmetry and different kinds of distortion. Such a phase is not detected at room temperature, and consequently, there cannot be macroscopic Nd, Pr segregation in the present sample. Within the resolution of the X-ray and neutron diffractometers, the room-temperature phase for $x = 0.25$ is thus homogeneous.

Using the neutron diffractometer G4.1, the NPD patterns of $Nd_{0.25}Pr_{0.25}Sr_{0.5}MnO_3$ were registered from room temperature down to 1.5 K in steps 10−20 K (Figure 2). A very complex evolution of crystal and magnetic structures was observed. At 300 and 280 K, there is a single paramagnetic phase of *Ibmm* symmetry as mentioned above. Below 270 K the patterns show a gradual transformation of the orthorhombic *Ibmm* phase to the tetragonal *I*4/*mcm* phase (characterized by antiphase tilting about the [001] direction—in Glazer's notation $a^0a^0c^-$).[24] The crystallographic transition remains incomplete, and the maximum population of the *I*4/*mcm* phase reaches 45% of the sample at 160 K.

On cooling below 160 K, the patterns show (see the doublet at 78°) a formation of a new low-temperature phase of the orthorhombic character. Compared to the high-temperature *Ibmm* phase, this new structure shows a marked contraction along the *c* axis, which points to an orientation of manganese e_g orbitals into the *ab* plane. Precise symmetry assignment is difficult because the data come from a medium resolution diffractometer and the sample is multiphasic. For the present refinements the *Ibmm* space group is used, but the true symmetry can be decreased to *Pbnm* (if a more complex tilt $a^-a^-c^+$ is settled) and eventually to a monoclinic $P112_1/m$ in a doubled cell along the *b* axis (if orbital order

(24) Glazer, A. M. *Acta Crystallogr., Sect. B* **1972**, *28*, 3384.

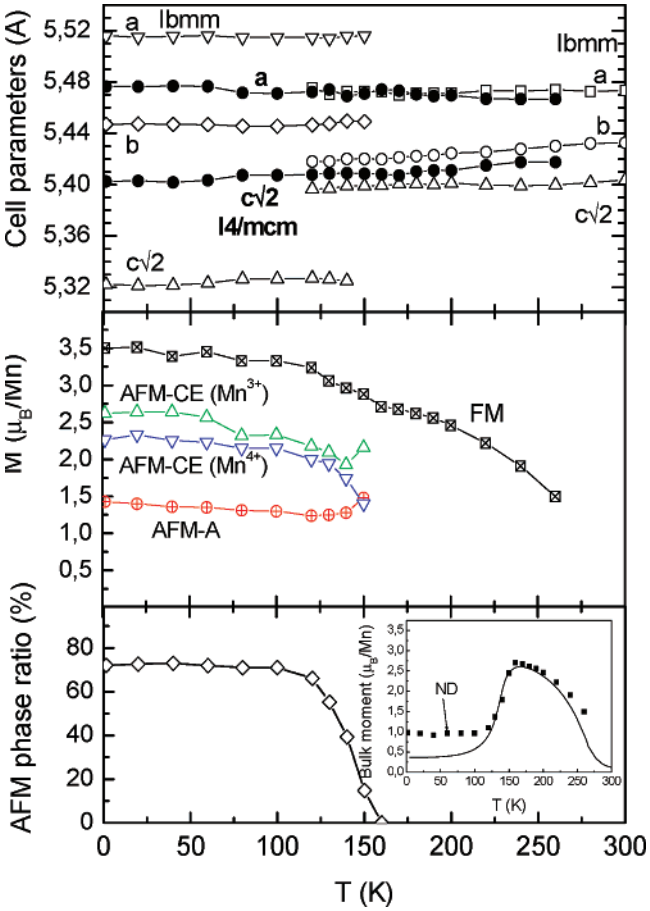

Figure 3. Temperature dependence of the lattice parameters observed for $Nd_{0.25}Pr_{0.25}Sr_{0.5}MnO_3$ (from G4.1 data). The middle panel shows a long range ordered FM moment averaged over the *I*4/*mcm* and high-temperature *Ibmm* phases and the CE and A-type AFM components averaged over the low-temperature *Ibmm* phase (for details see text). The lower panel shows the ratio of the strongly distorted AFM regions, and the inset gives the bulk magnetization calculated from the amount of FM regions and observed FM moments in neutron diffraction. The magnetization in the field of 5000 G (full line in the inset) is given for comparison.

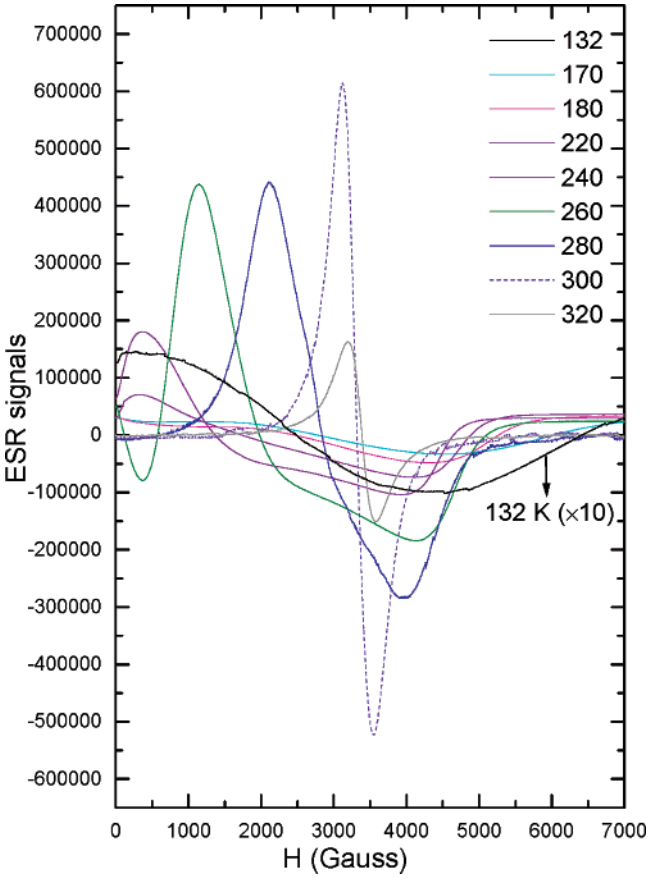

Figure 4. ESR spectra of the $Nd_{0.375}Pr_{0.125}Sr_{0.5}MnO_3$ sample at selected temperatures between 130 and 320 K.

is combined with the (Mn^{3+}/Mn^{4+}) charge order).[6,18] The results show that the high-temperature *Ibmm* phase completely vanishes at 120 K, the low-temperature *Ibmm* phase becomes dominant (72% of the sample), and the amount of the tetragonal *I*4/*mcm* is decreased to 28% of the sample.

The temperature dependence of unit cell parameters for the high- and low-temperature orthorhombic *Ibmm* phases and the tetragonal *I*4/*mcm* phase are shown in the upper panel of Figure 3. It is seen that the high-temperature *Ibmm* phase possesses a weak orthorhombic distortion with lattice parameters in a sequence $a > b > c\sqrt{2}$. The actual values at room temperature are $a = 5.4750(2)$ Å, $b = 5.4329(2)$ Å, $c = 7.6417(2)$ Å, and $V = 227.31$ Å.[3] The low-temperature *Ibmm* phase is distinguished by a much larger distortion $a > b \gg c\sqrt{2}$. The *I*4/*mcm* phase is characterized by a weak tetragonal elongation $c\sqrt{2}/a \approx 1.01$ that is associated with the $a^0a^0c^-$ tilt rather than with manganese e_g orbital polarization. The tilting angle of MnO_6 octahedra around the *c* axis is ±8.2°. At 140 K where all three crystallographic phases coexist in a ratio 40:38:22, an independent refinement shows $a = 5.4726(11)$ Å, $b = 5.4201(9)$ Å, and $c = 7.6354(20)$ Å for high-temperature *Ibmm*, $a = 5.5156(11)$ Å, $b = 5.4496(10)$ Å, and $c = 7.5309(16)$ Å for low-temperature *Ibmm*, and $a = 5.4090(7)$ Å and $c = 7.7345(24)$ Å for *I*4/*mcm*. The respective unit cell volumes are practically the same, 226.4 Å.[3] This suggests that the phase coexistence does not originate from a chemical inhomogeneity and should be related to an intrinsic separation or quenched disorder. Finally, at 1.5 K, the parameters for the low-temperature *Ibmm* phase make $a = 5.5160(6)$, $b = 5.4469(4)$, $c = 7.5269(9)$, and $V = 226.15(8)$ Å^3 and for the *I*4/*mcm* phase $a = 5.4025(7)$, $c = 7.7449(24)$, and $V = 226.05(8)$ Å^3.

As to the magnetic arrangement, an increase of the nuclear peak intensities at about 260 K (see the right-side inset of Figure 2) indicates a change of the paramagnetic state to a FM state. The FM order originates likely in the *I*4/*mcm* phase because much larger ordered moments could be attributed to that phase in a detailed Rietveld refinement at 220 K. The onset of bulk FM in the high-temperature *Ibmm* phase can be estimated to about 230 K (see also the anomaly in the resonance field in ESR experiments at the same temperature, Figure 6). At 160 K, the long-range ordered FM moments in both phases are comparable and make in average 2.7 μ_B. The spin orientation in the *I*4/*mcm* phase is along the tetragonal *c* axis for the *I*4/*mcm* phase, and it is expected to be perpendicular to the orthorhombic *c* axis in the *Ibmm* phase.

At about 150 K, additional peaks at low angles are observed (see the left-side inset) and attributed to the appearance of AFM states in the low-temperature *Ibmm* phase. At the same temperature, the FM contribution is partially suppressed due to decreased population of the high-

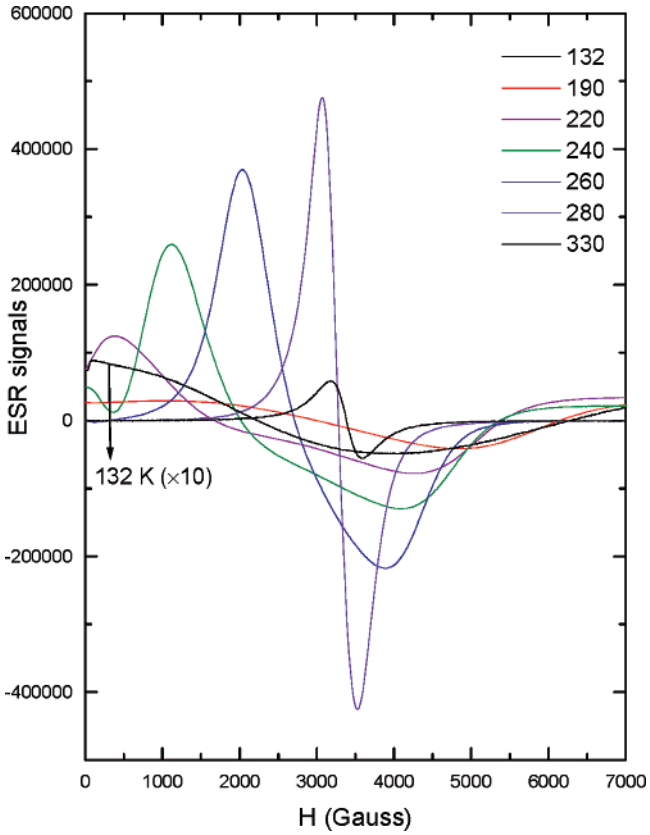

Figure 5. ESR spectra of the $Nd_{0.25}Pr_{0.25}Sr_{0.5}MnO_3$ sample at selected temperatures between 130 and 330 K.

temperature *Ibmm* and *I*4/*mcm* phases. A careful examination of patterns evidence a presence of two AFM arrangements in addition of the residual FM phase. One set of magnetic peaks corresponds to type A, and the other one can be attributed to type CE coupled with the Mn^{3+}/Mn^{4+} order. Both the A-type and CE-type AFM domains originate in the strongly distorted low-temperature *Ibmm* phase. The CE-type AFM order, which consists of FM zigzag chains running along the *b* axis and coupled antiferromagnetically in *a* and *c* directions, involves a further doubling of the *a* parameter with respect to the crystal structure. The CE-type ordered AFM moments are aligned along the *a* axis. The A-type AFM order consists of FM planes [001] coupled antiferromagnetically in the *c* direction. The A-type ordered Mn moments are oriented in the (001) plane, most likely along the *b* axis.

The refinement at 1.5 K shows that the average AFM moment per Mn atom makes 2.9 μ_B, pointing to a high degree of magnetic ordering in the CE and A-type domains of the low-temperature *Ibmm* phase (72% of the sample). Generally, the CE-type arrangement is more susceptible to defects than the A-type one, which means that the actual moments in A-type domains must be in the range 2.9−3.5 μ_B. With these limits we can estimate that CE-type regions comprise a minimum 54% of the sample with ordered moments $m(Mn^{3+}) = 3.05\ \mu_B$ and $m(Mn^{4+}) = 2.6\ \mu_B$, and A regions 18% with $m = 2.9\ \mu_B$; at a maximum they may comprise 60% with $m(Mn^{3+}) = 2.85\ \mu_B$ and $m(Mn^{4+}) = 2.5\ \mu_B$ and A regions 12% with $m = 3.5\ \mu_B$. The remaining 28% of the sample is formed by the *I*4/*mcm* phase of FM order. The observed moment makes 3.5 μ_B, which is exactly the full moment expected for the $Mn^{3.5+}$ ion.

The temperature dependence of the long-range ordered magnetic moments, determined by the refinement of neutron diffraction patterns, is shown in the middle panel of Figure 3. Here, the FM moments m_{FM} represent an average over the sum of high-temperature *Ibmm* and *I*4/*mcm* phases. The CE and A-type AFM values are components that refer to the total amount of the strongly distorted *Ibmm* phase. In particular, $\langle m_{CE} \rangle = 2.45\ \mu_B$ and $m_A = 1.45\ \mu_B$ at 1.5 K correspond to the average AFM moment per Mn atom given by $m_{AFM}^2 = \langle m_{CE} \rangle^2 + m_A^2$, that is, $m_{AFM} = 2.9\ \mu_B$ as mentioned above. Finally, the lower panel of Figure 3 shows the relative amount of the strongly distorted *Ibmm* phase with the occurrence of CE and A-type arrangements. In the inset, the bulk magnetization has been calculated from neutron diffraction data on m_{FM}. The values obtained are compared with the magnetization data in a field of 5000 G, measured on another sample of the same $Nd_{0.25}Pr_{0.25}Sr_{0.5}MnO_3$ composition. Some discrepancy at lower temperatures suggests that the amount of residual FM phase in the present compound may be sample and/or cooling-procedure dependent. In summary, the neutron diffraction study of $Nd_{0.25}Pr_{0.25}Sr_{0.5}MnO_3$ reveals a formation of a highly nonuniform state below the room temperature. First, there is a gradual segregation of FM regions of tetragonal symmetry on the background of the room-temperature orthorhombic PM phase. This process starts at $T_C = 260$ K. At about $T_{C2} = 230$ K, the bulk FM order is established also in the diminishing orthorhombic phase. The tetragonal and orthorhombic FM phases are found in half-to-half ratio at 160 K. Below 160 K, the orthorhombic phase quickly vanishes and the residual FM phase of the tetragonal symmetry coexists with AFM regions, realized in a new, strongly distorted orthorhombic perovskite cell. The presence of the CE-type and A-type AFM orderings ($T_N = 150$ K) suggests an occurrence of the (Mn^{3+}/Mn^{4+}) CO order in distinct parts of this strongly distorted phase. The observed temperature sequence of crystallographic and magnetic transitions leading to a magnetically and structurally heterogeneous ground state in a sample with single phase at room temperature is coherent with the following ESR measurements.

2. ESR Study. ESR spectra obtained between 300 and 130 K for $Nd_{0.5-x}Pr_xSr_{0.5}MnO_3$ ($x = 0.125$, 0.25) are shown in Figures 4 and 5. From these curves, the resonance field, the line width, and the DIN (which is proportional to the EMR susceptibility X_{EMR}) were extracted as a function of temperature (Figures 6 and 7). Similar behavior is observed for both samples.

As the temperature decreases from 330 to about 260 K, the spectra are characteristic for the PM state. They consist of a single line with a shape close to a Lorentzian derivative appearing for $g_{eff} = 2.007$ (resonance field $H_r = 3300$ G) irrespective of the temperature. The line width (ΔH_{pp}) goes through a minimum T_{min} at a temperature higher that $T_C = 260$ K ($T_{min} \approx 1.1T_C$) and only slightly increases as the temperature increases. The broadening below T_{min} is attributed to the existence of magnetic inhomogeneities which are created by the appearance of FM domains in the PM

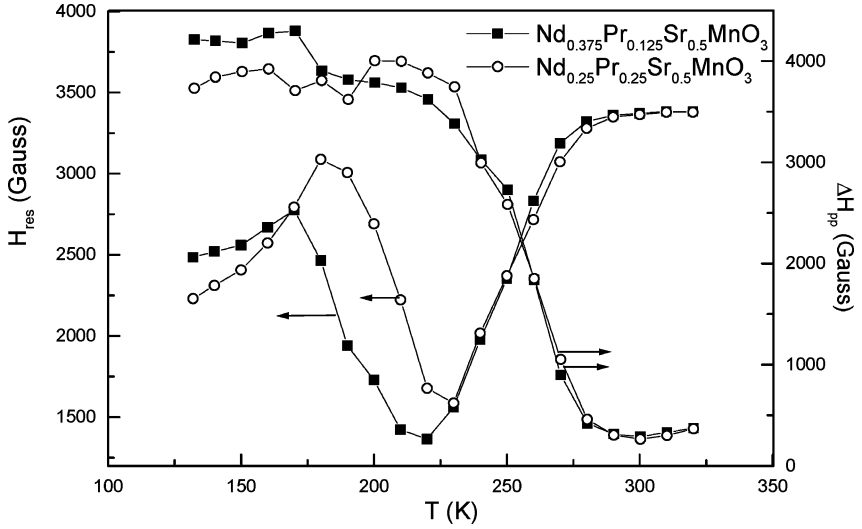

Figure 6. Temperature dependence of the line shape parameters for $x = 0.125$ and $x = 0.25$, resonance field (left y axis), and line width (right y axis).

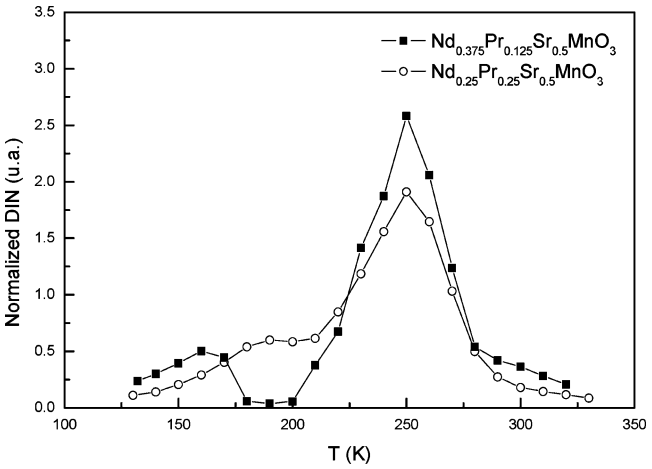

Figure 7. Temperature dependences of DINs (EMR susceptibility) for $x = 0.125$ and 0.25.

matrix. This behavior is similar to that described for other manganites with the FM ground state where the line width minimum can be shifted even up to $1.7T_C$. To explain this effect, different hypotheses were proposed like a relaxation bottleneck behavior[25,26] or a combined effect of Dzialozhinsky-Moriya and crystal field interactions.[27] In the "bottleneck" mechanism, the signal coming from Mn^{4+} ions with a Curie−Weiss behavior arises from the exchange coupling between the Mn^{3+} and Mn^{4+} subsystems,[25,26] whereas Huber et al. explain that the line width versus temperature behavior arises from the interplay of crystal field (single ion) anisotropy and antisymmetric Dzialozhinsky-Moriya exchange with isotropic superexchange between the Mn ions.[27]

Below 260 K, the ESR lines become asymmetrically broadened due to the crossover from the paramagnetic to FM resonance. The line width rapidly increases, and the resonance field (zero value of the derivative curves in Figures 4 and 5) is gradually shifted from 3300 G down to a minimum 1500 G at 220−230 K. Below this temperature, the line width remains very large, but the resonance field shifts in opposite direction, that is, to higher fields. At 170−180 K this trend culminates and a certain drop of the resonance field is detected at lower temperatures. It is worth mentioning that variations in the resonance field occur close to critical temperatures observed by neutron diffraction, onset of FM order in the tetragonal regions at $T_C = 260$ K, FM ordering in the orthorhombic phase at $T_{C2} = 230$ K, and formation of AFM phases at $T_N = 150$ K. In the literature, different hypotheses have been suggested to explain the behavior between T_C and T_N in the half-doped manganites. Rivadulla et al. argue that the FM phase in $La_{0.5}Ca_{0.5}MnO_3$ forms clusters that coexist with CO phase in PM state.[28] Indeed, the superposition of PM and FM signals between T_C and T_N was observed by ESR studies in $La_{0.5}Ca_{0.5}MnO_3$ and $Nd_{0.5}Sr_{0.5}MnO_3$, both with the CE-type AFM ground state.[29,30] As concerns half-doped manganites with the A-type AFM ground state and FM state at intermediate temperatures (e.g., $Pr_{0.5}Sr_{0.5}MnO_3$[7] or $Nd_{0.45}Sr_{0.55}MnO_3$[31]), there are no PM regions between T_C and T_N, but the FM phase is still not homogeneous as it exhibits A-type AFM spin fluctuations, detected by inelastic neutron scattering.[32] Our ESR curves between T_C and T_{C2} can be explained as a superposition of PM and FM signals due to the orthorhombic-tetragonal phase coexistence, observed for $Nd_{0.25}Pr_{0.25}Sr_{0.5}MnO_3$ by the neutron diffraction. The simple Lorentzian PM signal vanishes below T_{C2}, but the FM spectrum remains complex and is further changed on cooling. Detailed analysis of ESR spectra in this FM region is, however, difficult because of the polycrystalline character of our samples. More significant data obtained on single-crystal $Nd_{0.5}Sr_{0.5}MnO_3$ by Angapanne

(25) Shengelaya, A.; Zhao, G.; Keller, H.; Müller, K. A. *Phys. Rev. Lett.* **1996**, *77*, 5296.
(26) Shengelaya, A.; Zhao, G.; Keller, H.; Müller, K. A.; Kochelaev, B. I. *Phys. Rev. B* **2000**, *61*, 5888.
(27) Huber, D.; Alejandro, L. G.; Caneiro, A.; Causa, M.; Prado, T. F.; Tovar, M.; Oseroff, S. B. *Phys. Rev. B* **1999**, *60*, 12155.
(28) Rivadulla, F.; Freita-Alvite, M.; Lopez-Quintela, M. A.; Hueso, L. E.; Miguens, D. R.; Sande, P.; Rivas, J. *J. Appl. Phys.* **2002**, *91*, 785.
(29) Papavassiliou, G.; Fardis, M.; Milia, F.; Simopoulos, A.; Kallias, G.; Pissas, M.; Niarchos, D.; Ionnidis, N.; Dimitropoulos, C.; Dolinsek, J. *Phys. Rev. B* **1997**, *55*, 15000.
(30) Angappane, S.; Pattabiraman, M.; Rangarajan, G.; Sethupathi, K.; Sastry, V. S. *Phys. Rev. B* **2004**, *69*, 094437.
(31) Kuwahara, H.; Okuda, T.; Tomioka, Y.; Asamitsu, A.; Tokura, Y. *Phys. Rev. Lett.* **1999**, 82, 4316.
(32) Kawano-Furukawa, H.; Kajimoto, R.; Yoshizawa, H.; Tomioka, Y.; Kuwahara, H.; Tokura, Y. *Phys. Rev. B* **2003**, *67*, 174422.

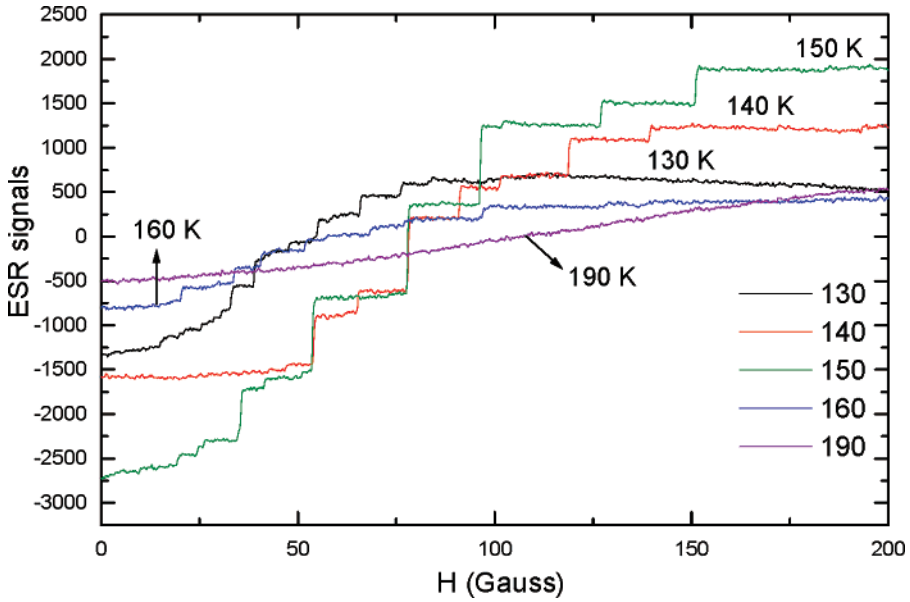

Figure 8. ESR spectra at low fields for $Nd_{0.25}Pr_{0.25}Sr_{0.5}MnO_3$.

et al. show that apart of the crystallographic phase coexistence and intrinsic effects like the above-mentioned AFM spin fluctuations there is an important role of magnetocrystalline anisotropy that influences the form of ESR spectra.[30]

DIN temperature dependence for both compositions of $Nd_{0.5-x}Pr_xSr_{0.5}MnO_3$ is shown in Figure 7. The DIN curve, which generally resembles the behavior of the AC susceptibility, exhibits a maximum at about 250 K corresponding to the FM transition, and a smaller bump at about 160 K for $x = 0.125$ and 180 K for $x = 0.25$ is seen. The ESR spectra below the formation of AFM phases at $T_N = 150$ should be attributed to residual FM domains. The signal is broad, and its intensity quickly decreases with temperature. The magnetic phase coexistence in this temperature range is further manifested in the ESR experiments at low fields (0 to 150 G). A careful observation of the ESR signal reveals a staircase profile for temperatures below $T_N = 150$ K (Figure 8). The position and number of steps do not appear at the same field upon cycling the magnetic field. On increasing the magnetic field above the threshold of spin flip, the spins tend to be aligned, and the steps disappear. A staircase profile was previously reported in the literature for metal alloys and or manganites.[22,33] It was interpreted as the results of either some kind of martensitic transformation or Barkhausen effect.[34,35] However, these scenarios are not clear because grain boundaries in ceramics could be intrinsic barriers for domain−wall movement. But, the appearance of jumps can be qualitatively explained by the competition between magnetic and electric phases. In some reports, the presence of steps was related to phase separation.[22,33] The $Nd_{0.25}Pr_{0.25}Sr_{0.5}MnO_3$ sample exhibits some FM domains coexisting with the CO AFM phase leading to a phase separated ground state. The strains within the samples that develop between the two phases due to their different unit cells play an important role. In such competition, the application of a magnetic field favors the growth of the FM phase at the expense of the AFM matrix.

Conclusion

Both the structural and the magnetic properties were investigated on polycrystalline material of mixed composition $Nd_{0.5}Sr_{0.5}MnO_3-Pr_{0.5}Sr_{0.5}MnO_3$ in the temperature interval from 300 to 1.5 K. Early studies on the end members report for $Nd_{0.5}Sr_{0.5}MnO_3$ the orthorhombic perovskite structure with a sequence of phase transitions PM → FM ($T_C \approx 260$ K) → charge ordered CE-type AFM ($T_N = T_{CO} \approx 160$ K) while $Pr_{0.5}Sr_{0.5}MnO_3$ exhibits tetragonal perovskite structure with transitions PM → FM ($T_C \approx 265$ K) → orbitally polarized A-type AFM ($T_N \approx 135$ K). In the mentioned CE and A-type ground states, only minor residual FM regions (few percent in maximum) have been detected. The present compounds with composition $Nd_{0.5-x}Pr_xSr_{0.5}MnO_3$ ($x = 0.125, 0.25$) are of the orthorhombic *Ibmm* symmetry at room temperature. The neutron diffraction has been performed on the sample with $x = 0.25$. The data evidence a gradual segregation of the FM phase of the tetragonal *I*4/*mcm* symmetry ($T_C \approx 260$ K), followed at $T_{C2} \approx 230$ K by FM ordering in the orthorhombic *Ibmm* phase. Finally, a new perovskite phase of large orthorhombic distortion and AFM ordering is formed at $T_N = 150$ K. As a result of these partial transitions, the compound occurs at low temperatures in a highly nonuniform state with coexistence in important ratios of the FM, charge ordered CE-type AFM and A type AFM regions, realized in two perovskite structures of distinct lattice distortions. The spins in respective regions are long range ordered as evidenced by high values of manganese moments calculated from the neutron diffraction data.

The ESR measurements are in coherence with the neutron diffraction results. The observed spectra and derived parameters (resonance field, line width, and integrated intensity) confirm the existence of four temperature regions. First is the PM region around the room temperature where

(33) Hébert, S.; Maignan, A.; Hardy, V.; Martin, C.; Hervieu, M.; Raveau, B. *Solid State Commun.* **2002**, *122*, 335.
(34) Podzorov, V.; Kim, B. G.; Kiryukhin, V.; Gershenson, M. E.; Cheong, S.-W. *Phys. Rev. B* **2001**, *64*, 140406.
(35) Barkhausen, H. *Z. Phys.* **1919**, 20, 401.

some signature for FM clusters can be indicated below ~1.1 T_C (T_C = 260 K). Next is a narrow region between T_C and T_{C2} where the tetragonal phase of FM order is formed at the expense of the orthorhombic PM phase. Below T_{C2}, the FM order is established in both crystallographic phases, and the amount of the tetragonal phase achieves a maximum close to 45% of the sample. Finally, below T_N, the CE and A-type AFM phases of strongly distorted perovskite structures are gradually formed while the orthorhombic FM phase quickly vanishes and FM order survives in tetragonal regions that make up about 28% of the sample at the lowest temperature.

CM070628+